JOURNAL OF CHEMICAL INFORMATION AND MODELING

Article

pubs.acs.org/jcim

Pharmacophore Assessment Through 3-D QSAR: Evaluation of the Predictive Ability on New Derivatives by the Application on a Series of Antitubercular Agents

Laura Friggeri,[§,†] Flavio Ballante,*[,§,‡] Rino Ragno,*[,‡] Ira Musmuca,[‡] Daniela De Vita,[†] Fabrizio Manetti,[○] Mariangela Biava,[†] Luigi Scipione,[†] Roberto Di Santo,[⊥,†] Roberta Costi,[⊥,†] Marta Feroci,[∥] and Silvano Tortorella[†]

[‡]Rome Center for Molecular Design and [⊥]Istituto Pasteur-Fondazione Cenci Bolognetti, [†]Dipartimento di Chimica e Tecnologie del Farmaco, Sapienza Università di Roma, P. le A. Moro 5, 00185 Rome, Italy

[○]Dipartimento di Biotecnologie, Chimica e Farmacia, Università degli Studi di Siena, Via Aldo Moro 2, I-53100 Siena, Italy

[∥]Dipartimento di Scienze di Base e Applicate per l'Ingegneria, Sapienza Università di Roma, Via Castro Laurenziano 7, I-00161 Rome, Italy

S *Supporting Information*

ABSTRACT: Pharmacophoric mapping is a useful procedure to frame, especially when crystallographic receptor structures are unavailable as in ligand-based studies, the hypothetical site of interaction. In this study, 71 pyrrole derivatives active against *M. tuberculosis* were used to derive through a recent new 3-D QSAR protocol, 3-D QSAutogrid/R, several predictive 3-D QSAR models on compounds aligned by a previously reported pharmacophoric application. A final multiprobe (MP) 3-D QSAR model was then obtained configuring itself as a tool to derive pharmacophoric quantitative models. To stress the applicability of the described models, an external test set of unrelated and newly synthesized series of R-4-amino-3-isoxazolidinone derivatives found to be active at micromolar level against *M. tuberculosis* was used, and the predicted bioactivities were in good agreement with the experimental values. The 3-D QSAutogrid/R procedure proved to be able to correlate by a single multi-informative scenario the different activity molecular profiles thus confirming its usefulness in the rational drug design approach.

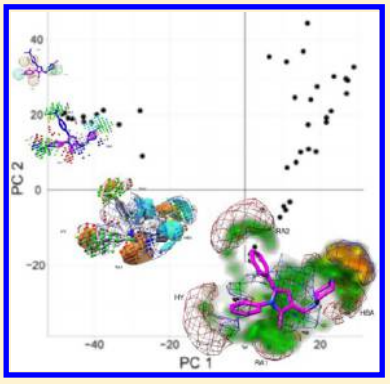

1. INTRODUCTION

Tuberculosis (TB), an infectious disease mainly caused by *Mycobacterium tuberculosis* (MTB), remains a major public health problem and causes ill-health among millions of people each year. TB ranks as the second leading cause of death from an infectious disease worldwide, after the human immunodeficiency virus (HIV-1). The 2012WHO Global tuberculosis report estimates there are almost 9 million new cases and 1.4 million TB deaths.[1] Moreover, two billion people are estimated to be latently infected with MTB, and 10% of them reactivate to active TB with major risk relative to immigrants from endemic areas, people with HIV-1 infection, and individuals with underlying diseases (silicosis, diabetes mellitus, malignant conditions).[2]

Currently, the standard treatment comprises: first line drugs, such as isoniazid (INH), pyrazinamide (PZA), ethambutol (EMB), and rifampin (RIF); and second line drugs, such as ethionamide (ETH), *p*-aminosalicylic acid (PAS), capreomycin, amynoglicosides, D-cycloserine (DCS), and fluoroquinolones.[3]

The required long-term drug treatment, due to the high persistence of MTB, combined with poor compliance of the patients, highly contributes to developing drug resistant strains, particularly multidrug-resistant (MDR, resistant at least to INH and RIF) and extensively drug-resistant (XDR, resistant at least to INH, RIF, and three of second line class of anti-TB drugs). Recently a more dangerous form of bacilli, named totally drug-resistant (TDR) showing in vitro resistance to all first- and second-line drugs tested have been isolated.[4,5]

To reduce this increasing problem, antitubercular drugs are used with specific therapeutic protocols under direct observation therapy short course (DOTS) conditions.[6]

The need for new shorter therapeutic regimens and new classes of drugs active on MDR, XDR, and TDR MTB drives pharmaceutical research to accelerate in the development process of new anti-TB drugs.[7] Continuing our research on anti-TB agents,[8,9] here we report the assessment of a previously reported pharmacophore model[10] through 3-D QSAutogrid/R, a recent introduced quantitative ligand-based design protocol.[11] The developed 3-D QSAR models were tested for their predictive ability on a series of new independently synthetized *R*-4-amino-3-isoxazolidinone derivatives **1a−e**, **2a−f**, and **3h,i** (Table 1). These compounds have been designed to evaluate the effects on antitubercular activity due by the introduction of acyl substituents on N(2) atom of oxoisoxazolidine ring and on amino group.

Received: March 1, 2013
Published: April 25, 2013

dx.doi.org/10.1021/ci400132q | *J. Chem. Inf. Model.* 2013, 53, 1463−1474

Table 1. *R*-4-Amino-3-isoxazolidinone Derivatives: Monocarbamates (1a−e), Dicarbamates (2a−f), and Amides (3h,i)

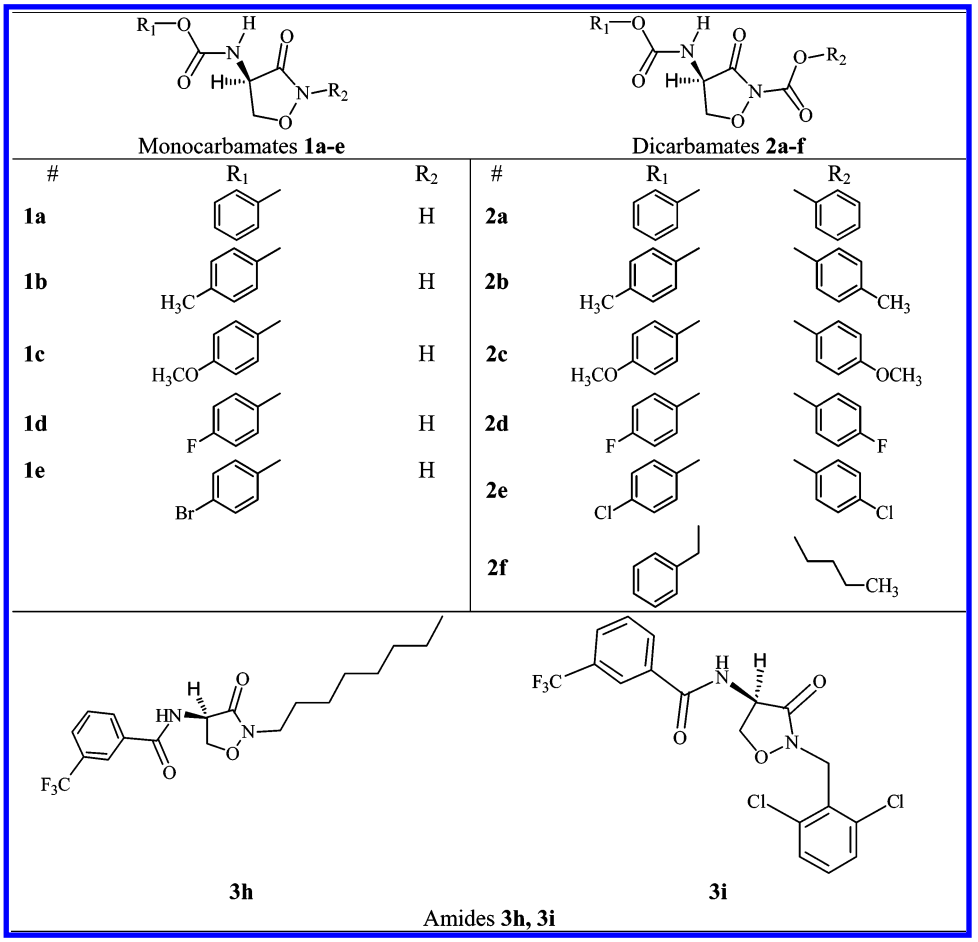

2. RESULTS AND DISCUSSION

2.1. Ligand-Based Design. A first pharmacophore model for anti-TB activity was previously developed by us[12] using a series of 32 imidazole derivatives with interesting antitubercular activity, adopting the HipHop[13] method. The final model was then optimized,[14] finally characterized by four pharmacophoric features as follows—a hydrogen bond acceptor feature (HBA), two aromatic ring features (RA1, RA2), and a hydrophobic feature (HY)—and applied recently to different antimycobacterial agents.[10,15] Even if this model is able to describe the needed structural properties for antitubercular activity and identify the possible antimycobacterial candidates within large molecular databases, it does not permit correlation of quantitative biological activity of the compounds with their structural features. This limitation is due to the fact that the model was obtained by application of the qualitative approach referred to as the common feature hypothesis generation method. In addition, as for the specific case of the newly synthesized monocarbamates (**1a−e**), dicarbamates (**2a−f**), and amides (**3h,i**) of *R*-4-amino-3-isoxazolidinone (Figure 1, discussion in the External Test Set Prediction Analysis paragraph), a proper evaluation may be difficult when a partial overlap of the investigated compounds with the defined pharmacophore areas is established. In this perspective the use of a three-dimensional quantitative approach is useful, and several 3-D QSAR partial least squares (PLS) models, characterized by a training set (Table 2, Table S1 for numeric reference) of 71 published antitubercular agents,[10,15−19] were built through the 3-D QSAutogrid/R[11] protocol: 8 monoprobe (see Supporting Information Table S5 for probes' definitions) 3-D QSAR PLS models were generated and optimized via the CAPP[11] procedure (Tables 3 and 4) and a final multiprobe (MPGRS)[11] model (Tables 5 and S5) was then derived to correlate the pharmacophoric features required for antitubercular activity with molecular structures. Activity data, originally determined as MIC (μg/mL) values, were transformed to pMIC values on molar basis.

Three of the best monoprobe 3-D QSAR models, A, HD, and NA (Table 4 and Supporting Information Figure S1), accounting for different interaction patterns, were selected for further analysis, and the relative 3-D plots were inspected (Figure 2, Figures S2−S4). A comparison between these plots and the original pharmacophoric model[14] was performed to check for spatial superposition of plot regions and pharmacophoric features (compare Figure 2A−C with D). Interpretation of the PLS-coefficients plots could be helped considering eq 1 where C_n is the C_{PLS} coefficient in the *n*th grid point, X_n is the actual field in the *n*th grid point, *Y* is the biological activity, and *n* is the number of grid points.

General equation for QSARs

$$Y = C_1X_1 + C_2X_2 + \ldots + C_nX_n + e \quad (1)$$

As addressed by eq 1, C_{PLS} coefficients provide both interpretation of training set data (explaining the relative influence of each grid point by means of size and sign) and prediction of test set molecules' biological activity, *Y* ; an

dx.doi.org/10.1021/ci400132q | J. Chem. Inf. Model. 2013, 53, 1463−1474

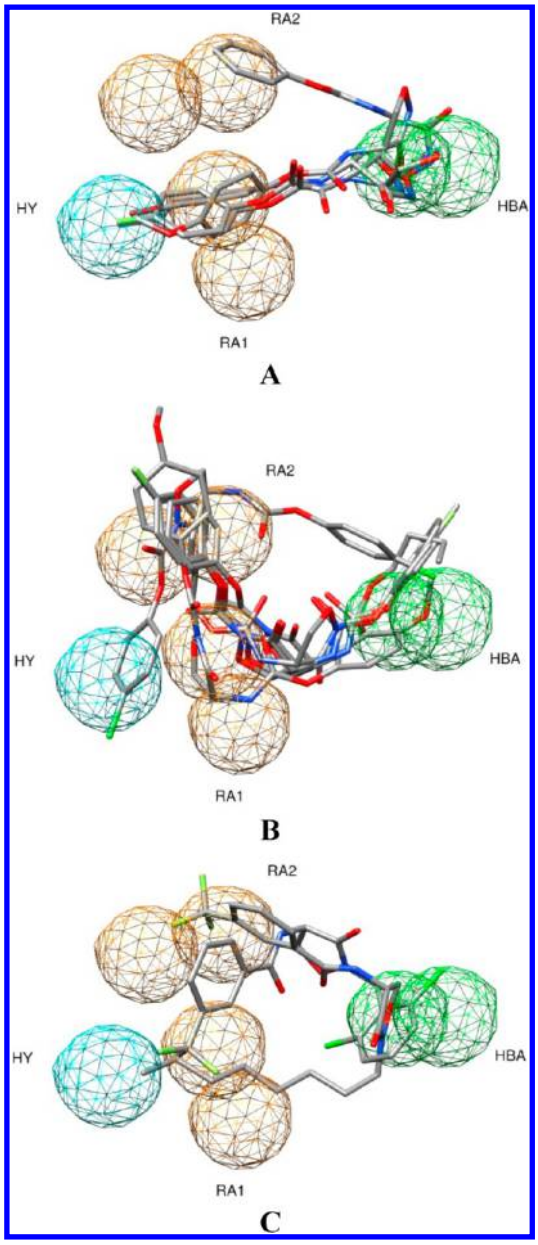

Figure 1. (A) Monocarbamates (**1a−e**). (B) Dicarbamates (**2a−f**). (C) Amides (**3h,i**) of D-4-amino-3-isoxazolidinone placed in the reported pharmacophoric model:[14] HY (hydrophobic feature), RA (aromatic feature), HBA (hydrogen bond acceptor feature). The four pharmacophoric features are color-coded according the original reference.

interaction characterized by a positive (repulsive) field X_n into a region with positive PLS-coefficient C_n will produce a positive effect ($C_n \times X_n$ product is positive), denoting a positive influence on Y (higher pMIC); the opposite is valid if the field or the PLS-coefficient have negative X_n or C_n, respectively. A positive effect (still considering pMIC activities) could be produced as well by a negative (attractive) field X_n into a region with negative PLS-coefficient C_n ($-C_n \times -X_n$ product is positive) and the opposite effect if the field or the PLS-coefficient have positive X_n or C_n, respectively.

As a result, four areas of the PLS-coefficients plots were distinguished over the N1, C2, C3, and C5 substituents of the pyrrole ring which overlap the pharmacophoric features HY, RA1, HBA, and RA2, respectively, thus suggesting a good agreement between QSAR and pharmacophoric models.

All monoprobe 3-D QSAR models clearly suggest that the presence of bulky groups as substituent at N1, C2, C5 is preferred, especially in N1 and C5 (HY and RA2 features). Moreover, the PLS-coefficient plots within thiomorpholines and methylpiperazinyl derivatives, (i.e., compounds **60** and **21** in Figure 2) and even more both PLS-coefficients and activity contribution plots (Supporting Information Figures S2−S4) show that at the C3 position steric features are required within certain limits. In particular, concerning the HBA feature, the HD model clearly shows that attractive interactions involving the sulfur of the thiomorpholine group of **60** (the most active compound, Figure S3A) increase the biological activity, while if these are missing or replaced by repulsive interactions, as for **21** (the least active compound), the biological effect decreases (Figure S3B). Therefore, a bulky group like thiomorpholinomethyl, also able to participate in electrostatic interactions, such as hydrogen bonds, is preferred at the C3 position. As for the structural features required for activity, the simultaneous analysis of PLS-loading and score plots were very useful to carry out the most relevant variables from the models (loading plots) and interpret the patterns seen in the score plots. Interesting is the case of the A probe model: starting from the first principal component (PC1), the presence of two clusters, differing each other for their conformational properties, is clearly showed in the score plot (Figure S5A). As shown in Figure S6 by superimposing the most influencing compounds (absolute higher score values) for each cluster to the PLS-loadings, the most important molecular feature in the PC1 space is related to both different spatial orientations and conformations. Light gray molecules, that are in the positive field cluster (positive PC1), had a higher activity and fill the lower part of the region between the RA2 and HBA features but not between RA1 and HBA. On the contrary, molecules with lower pMICs fill the area between the RA1 and HBA. Therefore a given derivative able to preferably occupy the region between the RA2 and HBA features should be endowed of a higher activity than a molecule filling the area between the RA1 and HBA. PC2 and PC3 respectively gave information about substituents at C3 (Figures S5B, S7, and S8), suggesting the presence of bulky groups in the upper areas between the RA2 and HBA and over the HBA features have a detrimental effect on the biological activity.

Application of Multi-Probe Guided Region-Variable Selection. By application of the Multi Probe Guided Region Selection (MPGRS package), as implemented in 3-D QSAutogrid/R,[11] a multiprobe (MP) 3-D QSAR model was derived, representing, to the best of our knowledge, the first quantitative pharmacophoric model able to correlate the structural features of pyrrole derivatives with their biological data. The optimal MP 3-D QSAR model was characterized by a $PC_{FL:SL}$ = 1:3,[11] and as previously reported,[11] its associated statistical coefficients (Table 5, Figure S9) were similar to those of the monoprobe models, but the interpretation was greatly enhanced. Applying a q^2 threshold value of 0.4, the most relevant MIF subregions were selected (Figure 3) to build the multiprobe MIF and the resulting MP model condensing into one all the suggestions retrieved by the analysis conducted on the monoprobe models. In particular, the MP PLS-loadings in association with the MP score plots identified the same conformational differences, addressed by the monoprobe models, as the most discriminating aspect in molecular clustering, for example: starting from $PC_{1:1}$ to $PC_{1:2}$ a similar clustering in the score plots and in meaning for the descriptors

dx.doi.org/10.1021/ci400132q | J. Chem. Inf. Model. 2013, 53, 1463−1474

Table 2. Structure and Antimycobacterial Activity against *M. tuberculosis 103471* of the Pyrrole Derivatives Used As a Training Set for the Generation of the 3-D QSAR Models

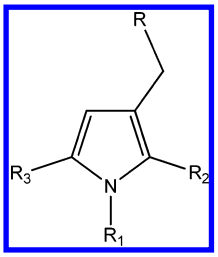

compd[a]	R[b]	R_1	R_2	R_3	pMIC[c]
1	B	2-F-Ph	CH_3	2-F-Ph	4.68
2	A	2-Cl-Ph	CH_3	2-F-Ph	5
3	B	2-Cl-Ph	CH_3	2-F-Ph	4.09
4	A	2-F-Ph	CH_3	2-Cl-Ph	5
5	B	2-F-Ph	CH_3	2-Cl-Ph	4.4
6	A	2-Cl-Ph	CH_3	2-Cl-Ph	5.02
7	B	2-Cl-Ph	CH_3	2-Cl-Ph	4.41
8	A	2-F-Ph	CH_3	α-naphthyl	4.11
9	B	2-F-Ph	CH_3	α-naphthyl	4.11
10	A	2-Cl-Ph	CH_3	α-naphthyl	4.13
11	B	2-Cl-Ph	CH_3	α-naphthyl	4.13
12	A	α-naphthyl	CH_3	2-Cl-Ph	4.13
13	B	4-F-Ph	CH_3	Ph	4.36
14	B	Ph	CH_3	4-F-Ph	4.36
15	A	4-Cl-Ph	CH_3	4-F-Ph	5.30
16	B	4-F-Ph	CH_3	4-F-Ph	4.47
17	A	4-F-Ph	CH_3	4-F-Ph	5.58
18	B	4-F-Ph	CH_3	4-Cl-Ph	5.30
19	A	4-F-Ph	CH_3	4-Cl-Ph	5.60
20	A	2-F-Ph	CH_3	Ph	4.66
21	B	2-F-Ph	CH_3	Ph	4.06
22	A	Ph	CH_3	2-F-Ph	4.96
23	B	Ph	CH_3	2-F-Ph	4.36
24	A	2-Cl-Ph	CH_3	Ph	4.38
25	B	2-Cl-Ph	CH_3	Ph	4.07
26	B	Ph	CH_3	2-Cl-Ph	4.07
27	A	α-naphthyl	CH_3	Ph	4.1
28	B	α-naphthyl	CH_3	Ph	4.09
29	A	Ph	CH_3	α-naphthyl	4.10
30	B	Ph	CH_3	α-naphthyl	4.09
31	B	Ph	CH_3	Ph	4.33
32	A	4-F-Ph	CH_3	2-Cl-Ph	5.00
33	B	4-F-Ph	CH_3	2-Cl-Ph	4.70
34	B	4-F-Ph	CH_3	2-F-Ph	4.08
35	A	4-F-Ph	CH_3	4-CH_3-Ph	5.98
36	B	4-F-Ph	CH_3	3-CH_3-Ph	4.37
37	A	4-F-Ph	CH_3	2-CH_3-Ph	4.98
38	B	4-F-Ph	CH_3	2-CH_3-Ph	4.07
39	A	4-F-Ph	CH_3	2,4-Cl_2-Ph	5.34
40	B	4-F-Ph	CH_3	2,4-F_2-Ph	5.00
41	A	2-Cl-Ph	CH_3	4-F-Ph	5.30
42	B	2-Cl-Ph	CH_3	4-F-Ph	5.00
43	B	2-F-Ph	CH_3	4-F-Ph	4.68
44	A	4-CH_3-Ph	CH_3	4-F-Ph	5.58
45	A	3-CH_3-Ph	CH_3	4-F-Ph	4.98
46	B	3-CH_3-Ph	CH_3	4-F-Ph	4.40
47	A	2-CH_3-Ph	CH_3	4-F-Ph	4.68
48	B	2-CH_3-Ph	CH_3	4-F-Ph	4.10
49	A	2,4-Cl_2-Ph	CH_3	4-F-Ph	5.64
50	B	2,4-Cl_2-Ph	CH_3	4-F-Ph	5.03
51	A	2,4-F_2-Ph	CH_3	4-F-Ph	5.30
52	B	2,4-F_2-Ph	CH_3	4-F-Ph	4.40
53	A	4-F-Ph	CH_3	4-C_2H_5-Ph	5.60
54	A	4-F-Ph	CH_3	4-*i*-propyl-Ph	6.21
55	A	4-C_2H_5-Ph	CH_3	4-F-Ph	5.30
56	A	4-C_3H_7-Ph	CH_3	4-F-Ph	5.61
57	A	4-Cl-Ph	CH_3	4-CH_3-Ph	5.90
58	A	4-Cl-Ph	CH_3	4-C_2H_5-Ph	6.22
59	A	4-Cl-Ph	CH_3	4-C_3H_7-Ph	6.23
60	A	4-Cl-Ph	CH_3	4-*i*-propyl-Ph	6.53
61	A	4-CH_3-Ph	CH_3	4-Cl-Ph	5.90
62	A	4-C_2H_5-Ph	CH_3	4-Cl-Ph	5.91
63	A	4-C_3H_7-Ph	CH_3	4-Cl-Ph	6.23
64	A	4-*i*-propyl-Ph	CH_3	4-Cl-Ph	6.23
65	B	4-Cl-Ph	C_2H_5	4-Cl-Ph	5.33
66	A	4-F-Ph	C_2H_5	4-CH_3-Ph	6.20
67	A	Ph	C_2H_5	Ph	5.26
68	A	Ph	C_2H_5	4-F-Ph	5.58
69	A	4-F-Ph	C_2H_5	Ph	5.28
70	A	2-F-Ph	C_2H_5	4-F-Ph	5.30
71	A	2-F-Ph	C_2H_5	2-F-Ph	5.00

[a]A = thiomorpholin-4-yl and B = 4-methylpiperazin-1-yl. [b]pMIC = $-\text{Log}[\text{MIC}(\mu\text{M}) \times 10^{-6}]$. [c]Compound enumeration was assigned on the basis of the original increasing numbering from the oldest to the most recent reference. Supporting Information Table S1 shows the connections between the new and original enumerations.

Table 3. CAPP Settings

min value	parameter[a]	max value	step
0	PCO	10	1.0
0	Zeroing	0.05	0.005
0	MSDCO	5	1

[a]PCO: positive cut off. Zeroing: zeroing of very low data points. MSDCO: minimum standard deviation cut off.

to those in the A monoprobe model was noticed (compare Supporting Information Figures S10−S12 and Figures S5−S7), confirming the above assumptions (effect of difference in spatial arrangement and conformation). The MP PLS-coefficient plot showed that the most important regions were spatially and chemically overlapping with the pharmacophoric model[14] (compare Figure 3B and D). Taking into account the probe type with the associated PLS-coefficient sign, bulky groups seemed to be required at the N1, C2, and C5 positions (positive coefficients); furthermore negative PLS-coefficients were spread in the proximity of these areas and chlorine and fluorine substituents are associated to activity enhancement, these additional areas can be related to some electrostatic molecular environment (Figure 3B and C) in agreement with the pharmacophoric model.[16,18] In addition, regarding the C3 position (in the lower part of HBA and slightly extended toward RA2) the model indicates that a limited steric repulsion is tolerated and electrostatic endowed groups could be profitable for the activity. Further information about the HBA feature was derived overlapping the clustered molecules (Figure S10B) with both PLS-loadings and PLS-coefficients at $PC_{1:3}$ (Figure 4A and B): the implementation of different probes (such as NA

dx.doi.org/10.1021/ci400132q | J. Chem. Inf. Model. 2013, 53, 1463−1474

Table 4. 3-D QSAutogrid/R PLS Model Statistical Results[a,b]

model	P	PC	r^2	q_{LOO}^2	q_{KSFCV}^2	r_{YS}^2	q_{YS}^2	V
1	A	3	0.92	0.86	0.85	0.36	−0.33	3758
2	C	3	0.92	0.86	0.85	0.37	−0.33	4492
3	HD	3	0.91	0.85	0.84	0.39	−0.31	1217
4	NA	3	0.91	0.86	0.85	0.31	−0.33	531
5	N	3	0.91	0.85	0.85	0.32	−0.30	477
6	OA	3	0.91	0.85	0.85	0.36	−0.33	658
7	e	4	0.88	0.78	0.76	0.40	−0.48	468
8	d	4	0.91	0.85	0.84	0.35	−0.44	4412

[a]CAPP process was applied. [b]P: Autogrid Probe. PC: optimal number of principal components/latent variables. r^2: conventional square-correlation coefficient. q_{LOO}^2: cross-validation correlation coefficient using the leave-one-out method. q_{KSFCV}^2: cross-validation correlation coefficient using the *k*-fold cross-validation with 5 random groups and 100 iterations. r_{YS}^2: average square-correlation coefficient obtained after Y-scrambling process using 100 iterations; q_{YS}^2: average cross-validation correlation coefficient using the leave-one-out method obtained after Y-scrambling process using 100 iterations. V: number of active variables.

and HD) suggested that the presence of bulky groups in the upper areas between the RA2 and HBA and over the HBA feature might have a detrimental effect on the biological activity; i.e. considering the methylpiperazinyl moiety (characterizing most of the negative clustered molecules, Figure 4B2) the methyl group fits the HD areas characterized by a negative PLS-coefficient, while the thiomorpholinomethyl moiety (that discriminate the positive clustered molecules, Figure 4B1) satisfies both steric and electrostatic features leading to higher activities. In this scenario the MP model was able to increase the resolution of the HBA region revealing an extra partial steric role.

External Test Set Prediction Analysis. The 8 3-D QSAutogrid/R monoprobe models were externally validated using the 13 newly synthesized monocarbamates (**1a−e**), dicarbamates (**2a−f**), and amides (**3h−i**) (Table 1). A fact must be emphasized: since the training set was composed only by pyrrole derivatives to directly compare the quantitative models with the original pharmacophoric assumptions, the resulting quantitative structure−activity relationships were based, mostly, on the characteristics of the scaffolds composing the training set. This may result in a limitation of the models to predict the activities of other molecular classes: in this case, specifically, a major difference between the two sets, training set and test set, was represented by the fact that the former was characterized by the pyrrole ring, which permits a quadruple branching able to satisfy simultaneously the different pharmacophoric areas; on the contrary, the compounds of the test set were characterized by a double branching. Despite this fact, and considering also that the test set molecules showed similar activity values (total pMIC activity range = 1.31 log unit), acceptable errors of prediction (SDEP coefficients all below the unit except for the d model) were obtained (Table 6); but an analysis focused only on the statistical SDEP values or experimental vs predicted plots (Figure S13) could be misleading. In fact, analyzing only the statistical results might seem that the PLS models had good predictive ability toward the isoxazolidinone derivatives, while considering only the experimental vs predicted plots the same conclusion could not be reached. In this case, it was helpful to analyze both of these pieces of information, together with the average absolute error of predictions (AAEP, Supporting Information Table S6), for each molecule from all the 3-D QSAR monoprobe models and finally their placement in the 3-D space of PLS-coefficients. Analyzing, for each test set molecule, the AAEP from all the eight monoprobe models stood out the good predictive capacity toward 10 of these, while for **1a**, **2c**, and **2e**, the AAEPs were 1.05, 1.50, and 1.72, respectively. These compounds were overpredicted, and this can be sought precisely in the dependence of the model from the training set congenerousness and from consequent inevitable alignment limitations. Furthermore **1a** was predicted more active than **1d** likely due to the fact that its isoxazolidinonic carbonyl group was perfectly superimposed to the training set most active compound (**60**) thiomorpholinic sulfur atom, showing how important was for the models the presence of a group capable to accept hydrogen bonds in the HBA space. It should be stressed, however, that such molecules (**1a**, **2c**, and **2e**), probably, would have been discarded by adopting the original pharmacophoric model;[14] in fact, compound **1a** misses the RA1 and HY features while RA2 and HBA are satisfied with the presence of a phenyl in R1 and carbonyl group of the isoxazolidinone ring, respectively; **2c** satisfies only the RA2 feature, and partially the HBA feature with the presence of the *p*-methoxyphenylic oxygen; **2e** accomplishes the HY and partially the RA1 feature; whereas all the 3-D QSAR models are able to frame their level of activity: for this reason and for the above considerations, the models show a good predictive ability although different scaffold endowed molecules were used as test set. As examples of the 3-D QSAR model application the most and least active monocarbamate derivatives (**1d** and **1a**, respectively) overlapped with the A probe model PLS-coefficients are depicted in Figure 5A, while the most and the least active dicarbamate molecules (**2d** and **2f**, respectively) are reported in Figure 5B. Despite the above considerations differences in experimental activities appears to be determined by a better overlap of the aromatic ring with the *p*-fluorine on the HY and RA2 regions. Analogously, the MP model predictions were in good agreement with those of the monoprobe models (Table 7). The 3-D QSAR MP plots showing the more and less active monocarbamates and dicarbamates derivatives (Figure 6) indicated the lack of a simultaneous coverage of the different regions addressed by the PLS-coefficients. However, as shown in Figure 6 was confirmed the importance of hydrophobic substituents in the HY and RA2 areas, which should determine the highest activities of **1d** and **2d**.

Table 5. MPGRS: Multi Probe Model Statistical Results

MPGRS 3-D QSAR							
$PC_{FL:SL}$[a]	r^2[b]	q_{LOO}^2[c]	q_{KSFCV}^2[d]	$SDEP_{LOO}$	$SDEP_{KSFCV}$	r_{YS}^2	q_{YS}^2
1:3	0.88	0.80	0.80	0.32	0.32	0.31	−0.31

[a]Optimal number of principal first level (FL) and second level (SL) components for the MPGRS model; [b]Conventional square-correlation coefficient. [c]Cross-validation correlation coefficient using the leave-one-out method. [d]Cross-validation correlation coefficient using the *k*-fold cross-validation with 5 random groups and 100 iterations.

dx.doi.org/10.1021/ci400132q | J. Chem. Inf. Model. 2013, 53, 1463−1474

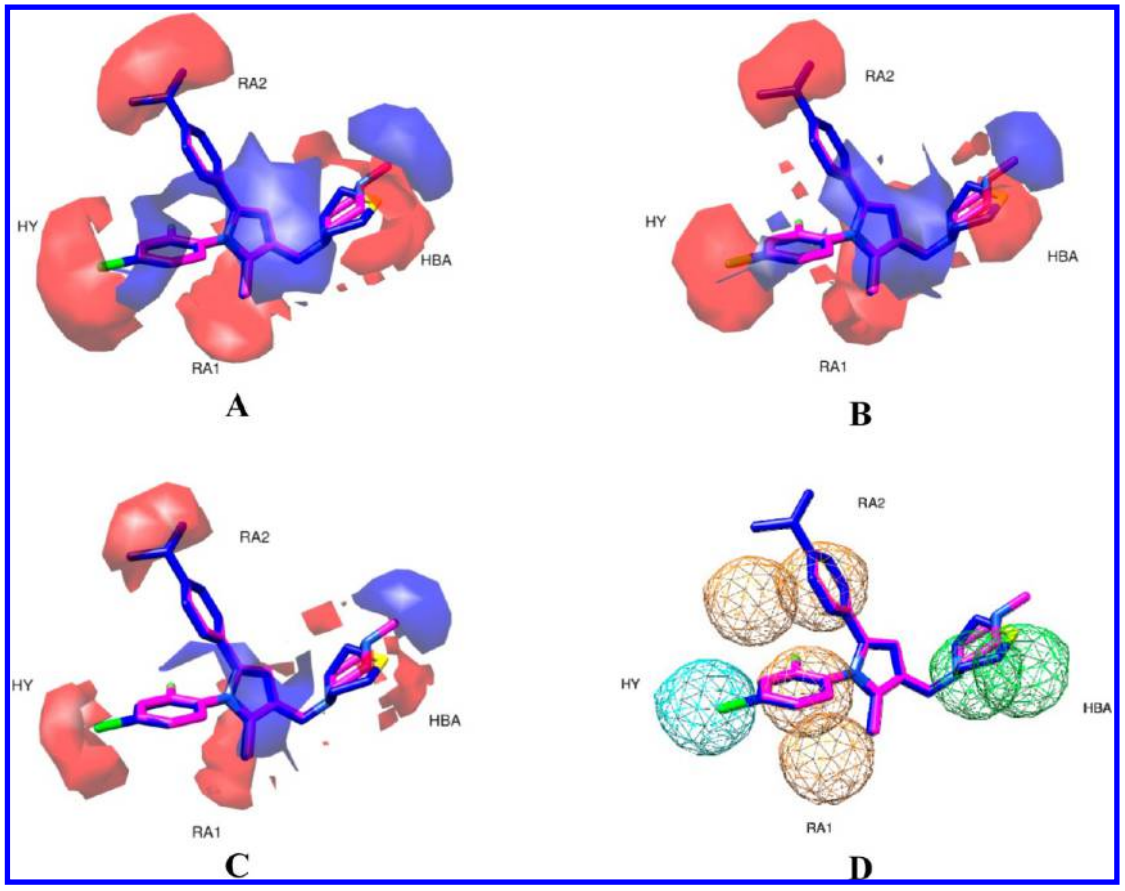

Figure 2. Most active (**60** in blue) and least active (**21** in magenta) compounds. (A) PLS-coefficients contour maps derived from A probe analysis (contour levels 80%; positive red, negative blue). (B) PLS-coefficients contour maps derived from HD probe analysis (contour levels 85%; positive red, negative blue). (C) PLS-coefficients contour maps derived from NA probe analysis (contour levels 75%; positive red, negative blue). (D) Pharmacophoric features derived from the original pharmacophoric model:[14] HY (hydrophobic feature), RA (aromatic feature), HBA (hydrogen bond acceptor feature).

2.2. Chemistry. The synthesis of compounds (**1a−e**) and (**2a−f**) was carried out modifying a literature procedure described by Stammer and co-workers,[20] by treatment of D-4-amino-3-isoxazolidinone in weakly alkaline media (1 M $NaHCO_3$) with the corresponding chloroformate to obtain both mono- and dicarbamate derivatives, as illustrated in Scheme 1.

The derivatives **1a−f** were prepared by regioselective acylation of the 4-amino group using the appropriate chloroformates at low temperature for short reaction time (0 °C for 3 h); then pure solids **1a−f** were obtained by acidification with 4 M HCl. Dicarbamate derivatives **2a−e** were synthetized dissolving the D-4-amino-3-isoxazolidinone in a basic solution at 0 °C and the selected chloroformates were dropwise added. **2a−e** gradually precipitate in 12 h from the acqueous solution.

The compound **2f** was obtained by treatment of **1f** with *n*-butylchloroformate in alkaline solution.

N-2-(alkyl)-4-amino-3-oxoisoxazolidinone **4h,i** were synthesized by an electrochemical reaction as previously reported.[21] Then crude **4h,i** were acylated with 3-trifluoromethyl benzoyl chloride in chloroform/TEA to give the amide derivatives **3h,i**.

In order to verify the racemization of the α carbon of D-4-amino-3-isoxazolidinone in the reaction conditions, we have analyzed by chiral HPLC the enantiopurity of (*R*)-**3h** and (*S*)-**3h**, obtained with the same synthetic procedure starting from (*R*)-4-amino-3-isoxazolidinone and (*S*)-4-amino-3-isoxazolidinone. Chiralpak Column IC 250 mm × 4.6 mm I.D. was used with *n*-hexane-2-propanol 75/25 (v/v) as eluent at flow rate of 1.0 mL/min at the temperature of 25 °C. In both the chromatogram of (*R*)-**3h** and (*S*)-**3h** an enantiomeric excess >99.0% was observed (Supporting Information Figure S15).

2.3. Biological Activity of Synthesized Compounds. The compounds were assayed for their antimycobacteria activity toward *M. tuberculosis* H37Rv (ATCC 27294). The minimal concentration inhibiting visible growth of mycobacteria was determinated for each compound.

Concerning the data reported in Table 8, only the acylation of 4-amino group and acylation or alkylation of N-2 of D-4-amino-3-isoxazolidinone influenced the antitubercular activity leading to a MIC value of 3.1 μg/mL (as in the case of **1d** and **2d**). Most of the tested compounds showed the same activity of the 4-amino-3-isoxazolidinone (32 μg/mL), while **1d** and **2d** were more active (3.1 μg/mL) and only the compound **3h** was less active (64 μg/mL).

3. CONCLUSION

In this paper we present the first application of a quantitative pharmacophoric model able to define and correlate the needed chemical characteristics with antitubercular activity of a previously reported class of antimycobacterial agents.[8,13−17] Eight 3-D QSAR monoprobe models and a multi probe (MP) model were built showing appreciable statistical coefficients and allowing an accurate definition of the structure−activity relationships on the basis of pyrrole derivatives used as training set. The MP 3-D QSAR model allowed defining the training set

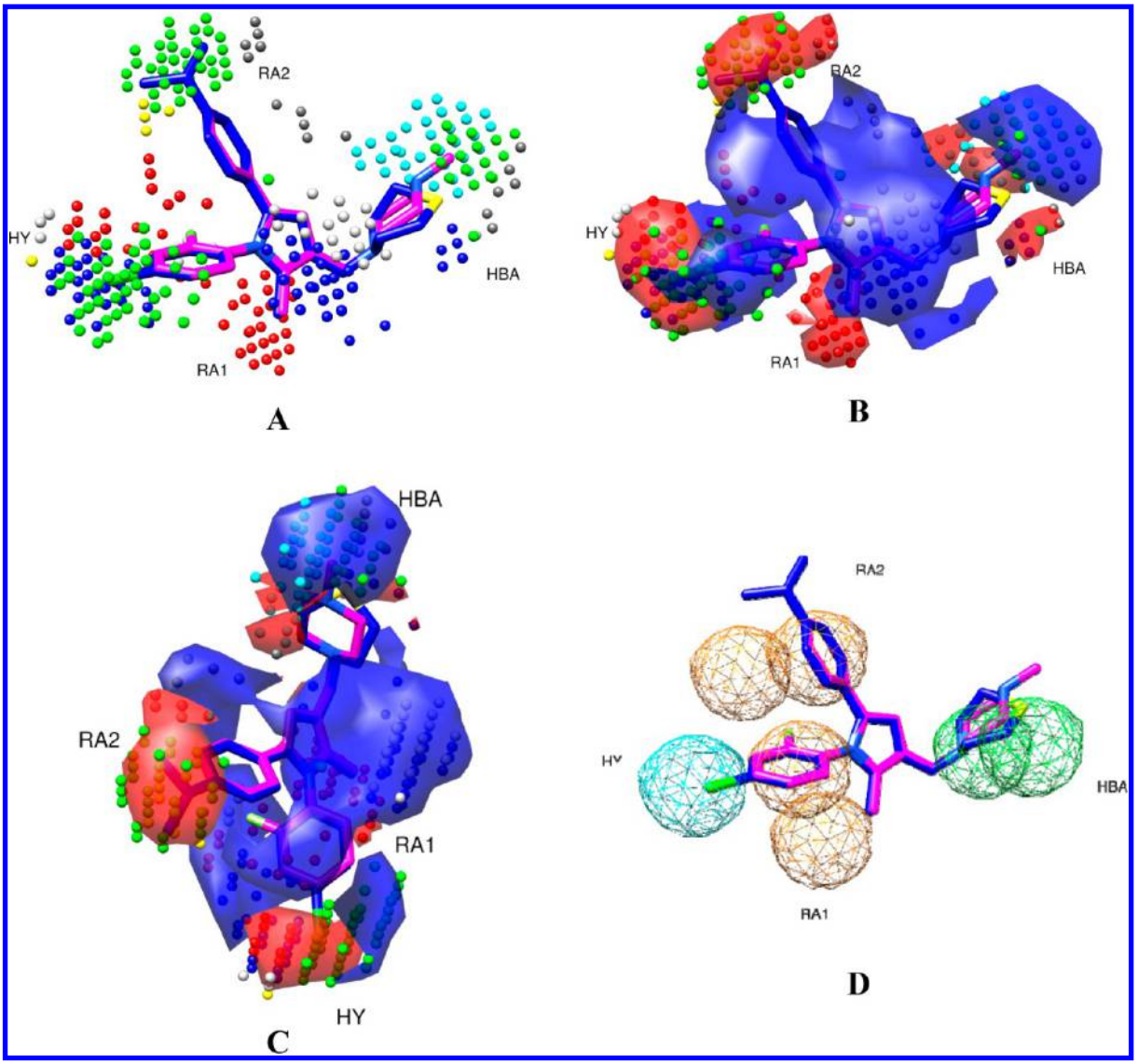

Figure 3. MPGRS. (A) Key points. The points are color-coded according to that reported in Supporting Information Table S5. (B) Key points with PLS-coefficients contour maps (contour levels: positive 85%, red; negative 95%, blue). (C) Top view, key points with PLS-coefficients solid contour maps (contour levels: positive 85%, red; negative 95%, blue). The most active (**60** in blue) and the least active (**21** in magenta) compounds are shown. (D) Pharmacophoric features derived from the original pharmacophoric model:[14] HY (hydrophobic feature); RA (aromatic feature), HBA (hydrogen bond acceptor feature).

molecular features and their three-dimensional positioning, configuring itself as a quantitative pharmacophoric model. Furthermore it was possible to elucidate the effect of conformational differences on the biological activity. As a further assessment the multi probe information was compared with the original pharmacophoric model, previously developed by us,[14] showing an high degree of correspondence.

Independently, a series of 13 isoxazolidinone derivatives **1**−**3** (Table 1) was synthesized and tested as new antitubercular compounds. The new compounds showed MIC values in the micromolar range. In particular among the monocarbamates and dicarbamates, derivatives **1d** and **2d** showed the higher biological activities. Although there are limitations due to structural differences between the molecules of the training set and those of derivatives **1**−**3**, the latters were used as an external test set to evaluate the models' predictive capabilities. All the 3-D QSAR models showed prediction errors (Tables 6 and 7), against these structurally unrelated molecules, with an acceptable degree of approximation.

The application of the models allowed to clarify the role of halogens and phenyl rings in **1a**−**e** and **2a**−**f**. Considering all these outcomes, the MP 3-D QSAR model could represent a useful tool for the design of new antitubercular drugs.

4. EXPERIMENTAL SECTION

4.1. Molecular Modeling and 3-D QSAR. All calculations used a 6 blade (8 Intel-Xeon E5520 2.27 GHz CPU and 24 GB DDR3 RAM each) cluster (48 CPU total) running Debian GNU/Linux 6.0 64 bit operating system. A series of 71 previously described pyrrole derivatives[10,15,19] were used to build 8 single probe and a multi probe 3-D QSAR models using the 3-D QSAutogrid/R procedure.[11] The obtained models were tested predicting the activities of the monocarbamates (**1a**−**e**), dicarbamates (**2a**−**f**), and amides (**3h,i**) of D-4-amino-3-isoxazolidinone derivatives.

dx.doi.org/10.1021/ci400132q | J. Chem. Inf. Model. 2013, 53, 1463−1474

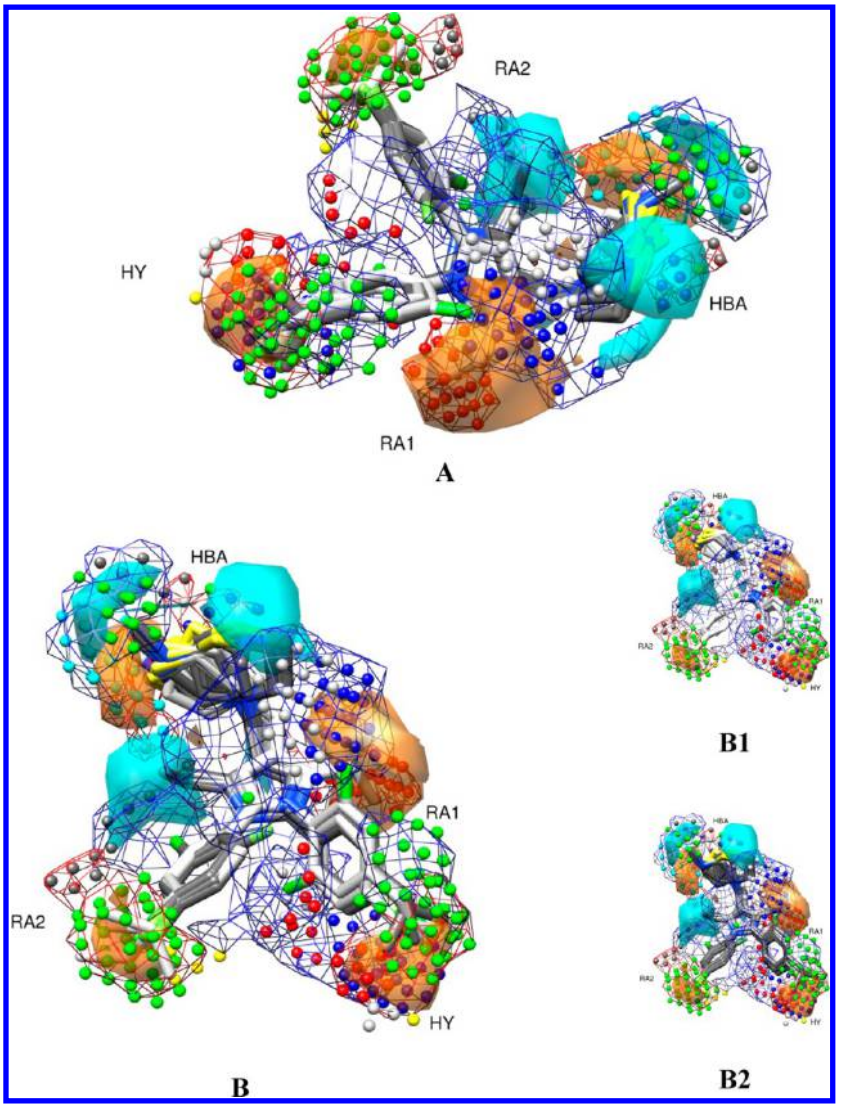

Figure 4. MPGRS. PLS-loadings contour maps at $PC_{1:3}$ (contour levels 75%; positive orange, negative cyan) with PLS-coefficients (mesh levels positive 85%, red; negative 95%, blue) and key points (see Table S5 for color coding). The ten most important molecules for each cluster are plotted and color-coded (compounds in the positive loading field in light gray; compounds in the negative loading field in dark gray): (A) side view; (B) frontal view; (B1) frontal view of only positive clustered molecules; (B2) frontal view of only negative clustered molecules. HY (hydrophobic feature), RA (aromatic feature), HBA (hydrogen bond acceptor feature).

Table 6. Test Set Predictions[a]

P	PC	$SDEP_{EXT}$
A	3	0.88
C	3	0.88
HD	3	0.81
NA	3	0.82
N	3	0.83
OA	3	0.84
e	4	0.90
d	4	1.51

[a]SDEP values considering the optimal PCs. P: AutoGrid Probe. PC: optimal number of principal components/latent variables. $SDEP_{EXT}$: standard deviation error of prediction (or root mean squared error of prediction, RMSEP) for the external test set.

Table 7. MPGRS: Multi Probe Model Test Set Predictions[a]

P	$PC_{FL:SL}$	$SDEP_{EXT}$
AutoGrid MP	1:3	0.89

[a]SDEP values considering the optimal first level and second level PCs. P: AutoGrid Multi-Probe. $PC_{FL:SL}$: optimal first level and second level PCs. $SDEP_{EXT}$: standard deviation error of prediction (or root mean squared error of prediction, RMSEP) for the external test set.

Training Set Selection. Starting from a training set composed by 90 pyrrole derivatives,[10,15,19] a selection based on inner relationship analysis were conducted to improve the robustness and prediction capabilities of the 3-D QSAR models: this leads to a final training set composed by 71 molecules (Table 2).

Alignment Rules. Training Set: Training set compounds were first submitted to a conformational search following a computational protocol previously described.[10] Next, each compound with its conformational models was aligned to the pharmacophoric model with the flexible fitting method implemented in Discovery Studio (version 3.0, Accelrys, Inc., San Diego, CA), that allows slight modification of each conformation to better fit the pharmacophore.

dx.doi.org/10.1021/ci400132q | J. Chem. Inf. Model. 2013, 53, 1463−1474

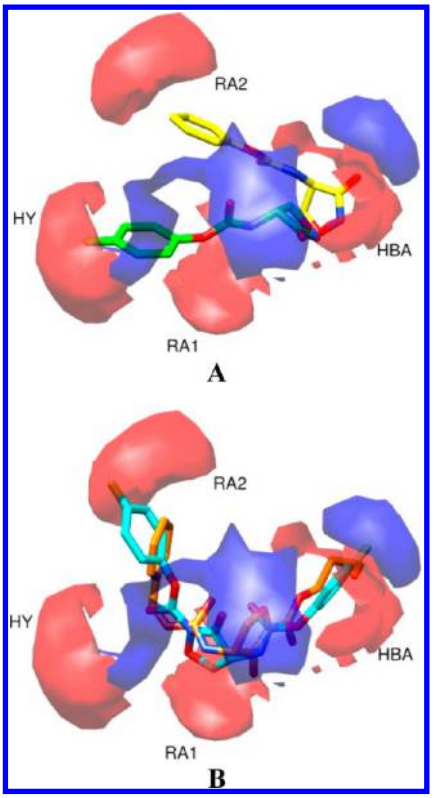

Figure 5. PLS-coefficients contour maps. (A) AutoGrid/R PLS-coefficients contour maps derived from the A probe analysis (contour levels 80%; positive red, negative blue; **1a** yellow; **1d** green); (B) AutoGrid/R PLS-coefficients contour maps derived from the A probe analysis (contour levels 80%; positive red, negative blue; **2d** cyan; **2f** orange). HY (hydrophobic feature), RA (aromatic feature), HBA (hydrogen bond acceptor feature).

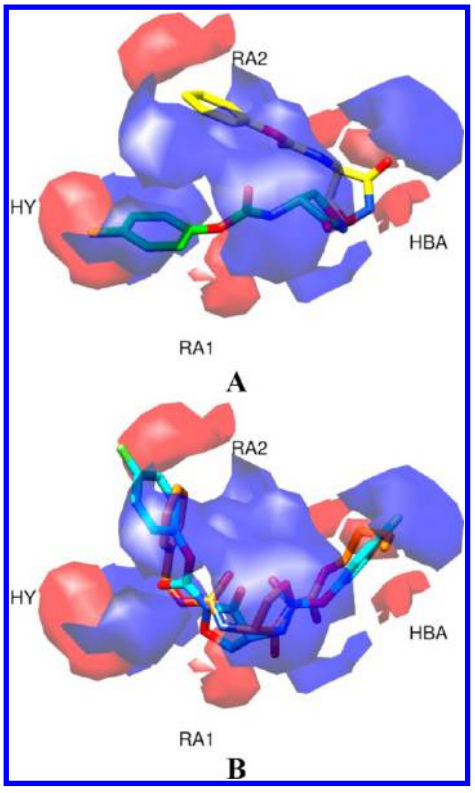

Figure 6. MPGRS. (A) PLS-coefficients contour maps at $PC_{1:3}$ (contour levels: positive 85%, red; negative 95%, blue. **1a**: yellow. **1d**: green). (B) PLS-coefficients contour maps at $PC_{1:3}$ (contour levels: positive 85%, red; negative 95%, blue. **2d**: cyan. **2f**: orange). HY (hydrophobic feature), RA (aromatic feature), HBA (hydrogen bond acceptor feature).

Test Set: The new 13 derivatives were aligned using the Surflex-Sim[22] software which has been chosen since it is a valuable tool in ligand-based drug discovery, free for academics, and its alignment process is based on morphological similarities. The query molecules' poses were optimized to the compounds used as training set to maximize 3-D similarity.

As shown in Supporting Information Figures S16 and S17 and Tables S9 and S10, similar results were obtained using the same alignment software (pharmacophoric alignment) adopted for the training set. The choice of Surflex alignment was not dictated by the improvement (although negligible respect the pharmacophoric one) in prediction, but by the fact that, in our view, this is a further confirmation of the robustness of the models, always taking into account the above limits. Indeed, using two different procedures of alignment, results are comparable and this should show that the predictive capability of the models is stable and in the specific case scarcely influenced. Further clarifications on the differences in prediction (as in the case of **1d** and **2d**) would be only speculative since the presence of similar activity values with a limited total pMIC activity range.

Strategies for different alignments were also tried leading to not consistent prediction supporting that the best alignment/prediction is that reported above.

Molecular Interaction Fields Calculation. As reported,[11] MIFs were generated using the AutoGrid Software (AutoDock Suite,[23] based on the AMBER united-atom Force Field) implemented in the 3-D QSAutogrid/R procedure, considering 8 different probes. Interaction energies between the selected probes and each molecule were computed using a grid spacing of 1 Å (Supporting Information Table S8). The *xyz* coordinates (in angstroms) of the grid rectangular box used for the computation were Xmin/Xmax = −9.828/12.172, Ymin/Ymax = −9.021/8.979, and Zmin/Zmax = −10.481/9.519.

Table 8. MIC Data for D-4-Amino-3-isoxazolidinone Derivatives

compd	MIC (μg/mL)[a]	pMIC[b]
1a	32	3.84
1b	32	3.87
1c	32	3.90
1d	3.1	4.89
1e	32	3.97
2a	32	4.03
2b	32	4.06
2c	32	4.10
2d	3.1	5.09
2e	32	4.11
2f	32	4.02
3h	64	3.78
3i	32	4.13

[a] *M. tuberculosis* H37Rv (ATCC 27294) was used. MIC values represent the minimal concentrations of compounds completely inhibiting visible growth of mycobacteria. [b] pMIC = −Log[MIC (μM) × 10^{-6}].

Statistical Analysis. Through the D2M package,[11] eight 3-D QSAR PLS models were built. During the model definition the

dx.doi.org/10.1021/ci400132q | J. Chem. Inf. Model. 2013, 53, 1463−1474

Scheme 1[a]

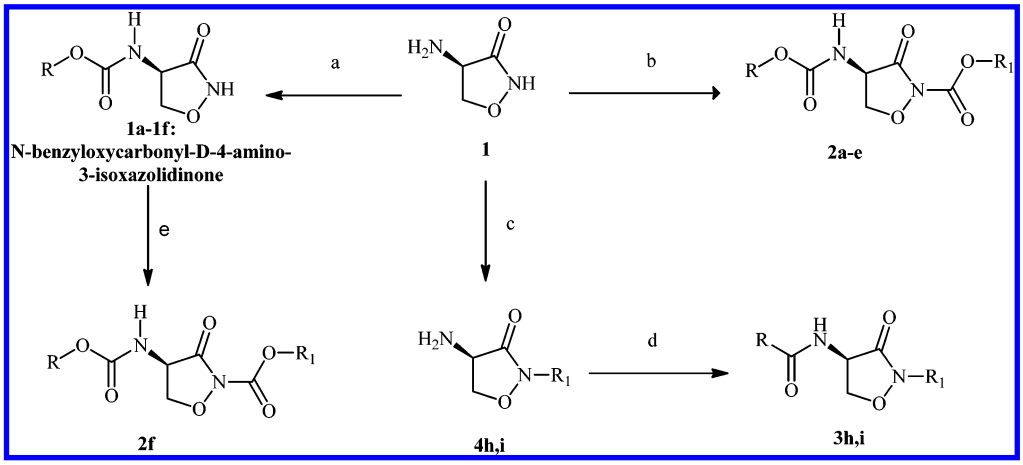

[a](a) R−O−CO−Cl, 1 M $NaHCO_3$, 0 °C 3 h, 4 M HCl; (b) R−O−CO−Cl, $NaHCO_3$, 0 °C, 15 h; (c) 0.1 M TEAHFP in CH_3CN, 30 mA cm^{-2}, D-4-amino-3-isoxazolidinone 1 eq (15 min), R_1−Br; (d) 3-CF_3−C_6H_4COCl, TEA, $CHCl_3$; (e) **1f**, *n*-Bu−O−CO−Cl, 1 M $NaHCO_3$, 0 °C, 24 h.

assessment of quality and robustness was conducted via two cross-validation (CV package)[11] procedures as follows: (1) leave-one-out (LOO) and (2) k-fold (KF, 5-random groups and 100 iterations) methodologies. Initially, the raw models (Supporting Information Table S2) were optimized through the Combinatorial Analysis of Pretreatment Parameters (CAPP package)[11] setting the pretreatment intervals as listed in Table 3, using the k-fold cross-validation with 5-random groups and 100 iterations and monitoring the q^2 and SDEP values. A total of 726 combinations, for each 3-D QSAR model, were processed using 5% sPRESS reduction[11] to select the optimal pretreatment combination and derive the pretreated PLS models; this led to an average q^2 K5FCV value increment equal to 14% (Supporting Information Table S4). Furthermore the scrambling approach, Y-scrambling, (package YS)[11] was applied to investigate the presence of chance correlations using 100 iterations. Considering the obtained good overall statistical coefficients together with the absence of chance correlations (Table 4, Supporting Information Table S3 and Figure S1), no further variable selection steps were performed. By the application of the MPGRS package,[11] a MP 3-D QSAR PLS model was then derived by selecting the most informative subregions for each of the eight considered probe; the same CV and scrambling procedures as those of the monoprobe models were performed and the optimal MP 3-D QSAR model was selected according to the $q_{FL:SL}^2$ values.[11] Similar statistical coefficients to those of the monoprobe models were obtained (Table 5, Supporting Information Figure S9) and no further variable selection were performed; finally the most relevant MIFs subregions were selected applying a q^2 threshold value of 0.4.

4.2. Chemistry. D-4-Amino-3-isoxazolidinone and all chloroformates were purchased from Sigma-Aldrich (Milano, Italy). All other reagents and solvents were of higher analytical grade. *N*-Benzyloxycarbonyl-D-4-amino-3-isoxazolidinone (**1f**) was prepared according to the procedure of Stammer et al.[20] Melting points were determined on Tottoli apparatus (Buchi) and are uncorrected. Vibrational spectra were recorded on a Spectrum One ATR Perkin-Elmer FT-IR spectrometer. ^1H and ^{13}C NMR spectra were acquired on a Bruker AVANCE-400 spectrometer at 9.4 T, in DMSO-d_6 or $CDCl_3$ at 27 °C; chemical shift values are given in δ (ppm) relatively to TMS as internal reference, coupling constants are given in hertz.

Mass spectra were recorded on a API-TOF Mariner by Perspective Biosystem (Straford, Texas, USA), and samples were injected by a Harvard pump using a flow rate of 5−10 μL/min, infused in the electrospray system, a TSQ quadrupole mass spectrometer by Thermofinnigan (San Jose, California, USA) operating in CH_4/CI conditions; samples were introduced in the CI source by a direct insertion probe. Elemental analyses were obtained by a PE 2400 (Perkin-Elmer) analyzer.

*General Procedure for Synthesis of Monocarbamates **1a−e**.* Compounds **1a−e** were prepared by a modified procedure described by Stammer et al.:[20] briefly, to 0.5 mmol of D-4-amino-3-isoxazolidinone, dissolved in 1.2 mL of aqueous 1 M $NaHCO_3$, cooled in an ice bath, 1.0 mmol of the corresponding chloroformate was added and the solution stirred for 3 h at 0 °C. Little amounts of precipitate that could be formed were filtered off, and the solution, kept to 0 °C, was acidified to pH 4 with 4 M aqueous HCl. After 30 min, the white fine precipitate was collected by centrifugation and washed with cold water. The collected carbamates **1a−e** were crystallized from water.

*Synthesis of (R)-Phenyl-(3-oxoisoxazolidin-4-yl)carbamate (**1a**).* **1a** was obtained as white crystalline solid in 75% yield, mp 148−149 °C. ^1H NMR (DMSO-d_6): 11.52 (1H, bs, D_2O exchange); 8.37 (1H, s, D_2O exchange); 7.38 (t, 2H, J = 8.56 Hz); 7.21 (t,1H, J = 7.58 Hz); 7.12 (d, 2H, J = 8.56 Hz); 4.65−4.60, (m, 1H); 4.56 (t, 1H, J = 9.78 Hz); 4.03 (t,1H, J = 8.32 Hz). ^{13}C NMR (DMSO-d_6): 170.5; 154.9; 151.4; 129.9; 125.9; 122.3; 72.2; 53.5. FT-IR (cm^{-1}): 3339, 1709, 1655. MS/ESI: $(M + H)^+$ 223.0730 (m/z).

*Synthesis of (R)-4-Methylphenyl-(3-oxoisoxazolidin-4-yl)-carbamate (**1b**).* **1b** was obtained as a white crystalline solid in 75% yield, mp 195−196 °C. ^1H NMR (DMSO-d_6): 11.54 (bs, 1H, D_2O exchange); 8.30 (s, 1H, D_2O exchange); 7.16 (d, 2H, J = 8.56 Hz); 6.99 (d, 2H, J = 8.56 Hz); 4.66−4.59 (m, 1H); 4.55 (t, 1H, J = 10.35 Hz); 4.02 (t, 1H, J = 8.32 Hz); 2.28 (s, 3H). ^{13}C NMR (DMSO-d_6): 169.9; 154.4; 148.5; 134.2; 129.6; 121.3; 71.6; 52.8; 20.3. FT-IR (cm^{-1}): 3305, 1709, 1654. MS/ESI: $(M + H)^+$ 237.0874 (m/z).

*Synthesis of (R)-4-Methoxyphenyl-(3-oxoisoxazolidin-4-yl)carbamate (**1c**).* **1c** was obtained as a white crystalline solid in 70% yield, mp 155−156 °C. ^1H NMR (DMSO-d_6): 11.45 (bs, 1H, D_2O exchange); 8.27 (s, 1H, D_2O exchange); 7.02 (d, 2H, J = 9.06 Hz); 6.91 (d, 2H, J = 9.06 Hz); 4.64−4.59

dx.doi.org/10.1021/ci400132q | J. Chem. Inf. Model. 2013, 53, 1463−1474

(m, 1H); 4.54 (t, 1H, J = 9.29 Hz); 4.02 (t, 1H, J = 9.29 Hz); 3.73 (s, 3H). ^{13}C NMR (DMSO-d_6): 170.0; 156.5; 154.6; 144.2; 122.5; 114.2; 71.6; 55.4; 52.8. FT-IR (cm^{-1}): 3314, 1709, 1655. MS/ESI: (M + H)$^+$ 253.0790 (m/z).

*Synthesis of (R)-4-Fluorophenyl-(3-oxoisoxazolidin-4-yl)-carbamate (**1d**).* **1d** was obtained as a white crystalline solid in 70% yield, mp 175−176 °C. ^{1}H NMR (DMSO-d_6): 11.54 (bs,1H, D_2O exchange); 8.39 (s,1H, D_2O exchange); 7.16 (d, 2H, J = 8.56 Hz); 6.98 (d,2H, J = 8.56 Hz); 4.68−4.63 (m,1H); 4.55 (t, 1H, J = 9.56 Hz); 4.03 (t,1H, J = 8.80 Hz). NMR (DMSO-d_6): 155.9 (d, J = 237.8 Hz); 154.1; 147.3; 123.9 (d, J = 7.32 Hz); 116.5; 116.0 (d, J = 22.7 Hz); 72.0; 53.4. FT-IR (cm^{-1}): 3320, 1712, 1699. MS/CI: (M + H)$^+$ 241 (m/z).

*Synthesis of (R)-4-Bromophenyl-(3-oxoisoxazolidin-4-yl)-carbamate (**1e**).* **1e** was obtained as a white crystalline solid in 75% yield, mp 180−181 °C. ^{1}H NMR (DMSO-d_6): 11.55 (bs,1H, D_2O exchange); 8.42 (s, 1H, D_2O exchange); 7.22 (d, 2H, J = 8.56 Hz); 7.16 (d, 2H, J = 8.56 Hz); 4.69- 4.62 (m, 1H); 4.56 (t,1H, J = 9.88 Hz); 4.04 (t, 1H, J = 8.80 Hz). ^{13}C NMR (DMSO-d_6): 170.0; 156.5; 154.6; 144.2; 122.5; 114.2; 71.6; 52.8. FT-IR (cm^{-1}): 3330, 1715, 1705. MS/CI: (M + H)$^+$ 302 (m/z).

*General Procedure for Synthesis of Dicarbamates **2a**−**f**.* A 50 mg (0.5 mmol) portion of D-4-amino-3-isoxazolidinone were dissolved in 1.2 mL of aqueous 1 M $NaHCO_3$ and cooled at 0 °C, and 1.0 mmol of the corresponding chloroformate was added; the solution was stirred for 15 h. The obtained precipitates were collected by centrifugation, washed three times with 2 mL of water, and dried under reduced pressure to give compounds **2a**−**f** subsequently crystallized from benzene.

*Synthesis of (R)-Phenyl-3-oxo-4-[(phenoxycarbonyl)-amino]isoxazolidine-2-carboxylate (**2a**).* **2a** was obtained as a white crystalline solid in 85% yield, mp 159−160. ^{1}H NMR (DMSO-d_6): 8.58 (bs, 1H, D_2O exchange); 7.47 (t, 2H, J = 7.83 Hz); 7.41 (t, 2H, J = 7.58 Hz); 7.33 (t, 1H, J = 6.48 Hz); 7.24 (d, 2H, J = 7.83 Hz); 7.23 (d, 1H, J = 6.70 Hz); 7.16 (d, 2H, J = 7.58 Hz); 5.03- 4.97 (m,1H); 4.80 (t, 1H, J = 10.15 Hz); 4.31 (t, 1H, J = 8.68 Hz). ^{13}C NMR (DMSO-d_6): 166.4; 154.1; 150.6; 149.5; 145.7; 129.8; 129.4; 126.6; 125.4; 121.6; 121.4; 69.8; 53.0. FT-IR (cm^{-1}): 3344, 1789, 1736, 1713; MS/ESI: (M + H)$^+$ 343.0914 (m/z).

*Synthesis of (R)-4-Methylphenyl-4-{[(4-methylphenoxy)-carbonyl]amino}-3-oxoisoxazolidine-2-carboxylate (**2b**).* **2b** was obtained as a white crystalline solid in 75% yield, mp 169−170 °C. ^{1}H NMR (DMSO-d_6): 8.48 (bs,1H, D_2O exchange); 7.25 (d, 2H, J = 7.83 Hz); 7.19 (d, 2H, J = 7.58 Hz); 7.11 (d, 2H, J = 7.83 Hz); 7.01 (d, 2H, J = 7.58 Hz); 5.01−4.94 (m,1H); 4.78 (t, 1H, J = 10.55 Hz); 4.29 (t, 1H, J = 8.69 Hz); 2.31 (s, 3H); 2.29 (s, 3H). ^{13}C NMR (DMSO-d_6): 166.4; 154.3; 148.4; 145.8; 147.3; 135.9; 134.5; 130.1; 129.7; 121.3; 121.1; 69.8; 53.0; 20.4; 20.3. FT-IR (cm^{-1}): 3339, 1788, 1737, 1713. MS/ESI: (M + H)$^+$ 371.1085 (m/z).

*Synthesis of (R)-4-Methoxyphenyl-4-{[(4-methoxyphenoxy)-carbonyl]amino}-3-oxoisoxazolidine-2-carboxylate (**2c**).* **2c** was obtained as a white crystalline solid in 70% yield, mp 144−145 °C. ^{1}H NMR (DMSO-d_6): 8.45 (1H, bs, D_2O exchange); 7.16 (d, 2H, J = 7.83 Hz); 7.06 (d, 2H, J = 7.58 Hz); 6.98 (d, 2H, J = 7.83 Hz); 6.93 (d, 2H, J = 7.58 Hz); 5.02−4.95 (m, 1H); 4.77 (t, 1H, J = 10.27 Hz); 4.28 (t, 1H, J = 9.23 Hz); 3.76 (s, 3H); 3.75 (3H, s). ^{13}C NMR (DMSO-d_6): 166.3; 157.3; 156.6; 156.5; 154.5; 144.0; 142.8; 122.5; 122.3; 114.6; 114.3; 69.8; 55.4; 55.3; 53.0. FT-IR (cm^{-1}): 3346, 1790, 1731, 1715. MS/ESI: (M + H)$^+$ 403.1017 (m/z).

*Synthesis of (R)-4-fluorophenyl-4-{[(4-fluorophenoxy)-carbonyl]amino}-3-oxoisoxazolidine-2-carboxylate (**2d**).* **2d** was obtained as a white crystalline solid in 75% yield, mp 179−180°. ^{1}H NMR (DMSO-d_6): 8.65 (bs, 1H, D_2O exchange); 7.50 (d, 2H, J = 8.80 Hz); 7.44 (d, 2H, J = 8.80 Hz); 7.29 (d, 2H, J = 8.80 Hz); 7.18 (d, 2H, J = 8.80 Hz); 5.03−4.97 (m, 1H, Hz); 4.79 (t, 1H, J = 10.52 Hz); 4.31 (t, 1H, J = 8.32 Hz). ^{13}C NMR (DMSO-d_6): 166.8; 160.0 (d, J = 243.1 Hz); 159.5 (d, J = 242.0 Hz); 154.6; 147.2 (d, J = 2.7 Hz); 146.2; 146.0 (d, J = 2.7 Hz); 123.9; 123.8 (d, J = 8.7 Hz); 116.9 (d, J = 23.6 Hz); 116.4 (d, J = 23.2 Hz); 70.2; 53.5. FT-IR (cm^{-1}): 3350, 1740, 1735, 1720. MS/CI: (M + H)$^+$ 379 (m/z).

*Synthesis of (R)-4-Chlorophenyl-4-{[(4-chlorophenoxy)-carbonyl]amino}-3-oxoisoxazolidine-2-carboxylate (**2e**).* **2e** was obtained as a white crystalline solid in 75% yield, mp 160−161 °C. ^{1}H NMR (DMSO-d_6): 8.65 (bs, 1H, D_2O exchange); 7.52 (d, 2H, J = 8.32 Hz); 7.45 (d, 2H, J = 8.32 Hz); 7.18 (d, 2H, J = 8.28 Hz); 7.15 (d,2H, J = 8.28 Hz); 5.01−4.97 (m, 1H); 4.80 (t, 1H, J = 9.52 Hz); 4.30 (t, 1H, J = 8.32 Hz). ^{13}C NMR (DMSO-d_6): 167.3; 159.7; 159.6; 155.1; 155.0; 147.7; 147.6; 124.4; 124.3; 117.5; 116.8; 70.7; 53.9. FT- IR (cm^{-1}): 3330, 1740, 1730, 1725. MS/CI: (M + H)$^+$ 412 (m/z).

*Synthesis of (R)-butyl-4-{[(benzyloxy)carbonyl]amino}-3-oxoisoxazolidine-2-carboxylate (**2f**).* A 0.5 mmol portion of *N*-benzyloxycarbonyl-D-4-amino-3-isoxazolidinone **1f** were dissolved in 2 mL of 1 M acqueous $NaHCO_3$; at 0 °C and 1.0 mmol of *n*-butylchloroformate was added. The resulting suspension was stirred at room temperature for 24 h. The obtained white crystalline solid was separated by centrifugation, washed with cold water, dried, and crystallized from benzene. Mp 170−174 °C; yield 75%. ^{1}H NMR (DMSO-d_6): 7.35 (s, 5H); 5.06 (s, 2H); 4.87−4.80 (m, 1H); 4.62 (t,1H, J = 8.08 Hz); 4.12 (t, 2H, J = 6.12 Hz); 4.10 (t, 1H, J = 9.4 Hz); 1.61 (m, 2H); 1.35 (m, 2H,); 0.88 (t, 3H, J = 7.90 Hz). ^{13}C NMR (DMSO-d_6): 167.3; 158.0; 148.3; 143.4; 129.1; 127.6; 127.4; 66.3; 65.9; 65.2; 63.9; 31.1; 19.4; 14.4.FT- IR (cm^{-1}): 3330, 1720, 1715, 1696. MS/CI: (M + H)$^+$ 336 (m/z).

*Synthesis of Amide Derivatives **3h,i**.* The cyanomethyl anion was generated by electrochemical reduction of anhydrous acetonitrile as previoulsly reported.[21] Anhydrous acetonitrile, containing 0.1 M tetraehtylamoniumesafluoro phosphate (TEAHFP) was electrolized, in N_2 atmosphere, at 30 mA cm^{-2} current until 1.0 F/mol was consumed (calculated relative to D-4-amino-3-isoxazolidinone); thereafter, 1.0 mmol of D-4-amino-3-isoxazolidinone were added and the solution stirred for 15 min. A 1.0 mmol portion of alkyl-bromide was added, and the solution was stirred for 1.5 h at room temperature . Removal of the solvent under reduced pressure gave a crude solid that was extracted with three portions of Et_2O, and the combined organic extracts were dried over anhydrous Na_2SO_4 and evaporated under reduced pressure to give a crude residue that was used, without further purification, for the synthesis of amides **3h,i**.

The crude residue (**4h** or **4i**) was dissolved in 20 mL of $CHCl_3$ and 1.2 mmol of TEA and 1.2 mmol of 3-(trifluoromethyl)-benzoyl chloride were added. The obtained solution was stirred at room temperature for 24 h. The solution was washed with saturated Na_2CO_3, dried over anhydrous Na_2SO_4, and removed under reduced pressure; the obtained residue was purified on silica gel column chromatography to afford pure **3h** and **3i**.

N-[2-(*n*-Octyl)-3-oxoisoxazolidin-4-yl]-3-(trifluoromethyl)-benzamide (**3h**) was purified on silica gel column (CH_2Cl_2/ethyl acetate, 9:1). Mp 95−96 °C; yield 70%. ^{1}H NMR (DMSO-d_6): 9.28 (bs,1H, D_2O exchange); 8.22 (m, 1H, J = 1.78 Hz); 8.18 (dd,1H, J = 7.71 Hz, J = 1.58 Hz); 7.95 (dd, 1H,

dx.doi.org/10.1021/ci400132q | J. Chem. Inf. Model. 2013, 53, 1463−1474

J = 7.91 Hz, J = 2.09 Hz); 7.74 (m, 1H); 5.09 (m,1H, J = 10.15 Hz); 4.61 (t,1H, J = 8.56 Hz); 4.11 (t, 1H, J = 8.68 Hz); 3.50 (d, 2H, J = 7.25 Hz); 1.56 (m, 2H); 1.26 (m, 10H); 0.85 (3H, t, J = 7.00 Hz). ^{13}C NMR (DMSO-d_6): 166.8; 165.4; 134.7; 132.1; 130.3; 130.0 (q, J = 32.4 Hz); 128.7; 125.8; 124.4; 70.2; 52.3; 45.2; 31.7; 29.0; 28.9; 26.8; 26.5; 22.5; 14.4. FT- IR (cm^{-1}): 3301, 1671, 1662. MS/CI: $(M + H)^+$ 387 (m/z).

N-[2-(2,6-Dichlorobenzyl)-3-oxoisoxazolidin-4-yl]-3-(trifluoromethyl)benzamide (**3i**) was purified on silica gel column (CH_2Cl_2/ethyl acetate, 9:1). Mp 162−164 °C; yield 75%. ^{1}H NMR (DMSO-d_6): 7.99 (bs, 1H, D_2O exchange); 7.80 (m, 1H, J = 1.58 Hz); 7.74 (dd, 1H, J = 7.55 Hz, J = 1.68 Hz); 7.59 (dd, 1H, J = 6.77 Hz, J = 1.98 Hz); 7.37 (m, 1H); 7.27 (t, 2H, J = 6.30 Hz);7.24 (d, 2H); 5.15 (s, 2H); 4.97 (m, 1H, J = 9.87 Hz); 4.87 (dd,1H, J = 8.33 Hz); 3.98 (t, 1H, J = 8.68 Hz). ^{13}C NMR (DMSO-d_6): 166.6; 166.1; 136.9; 133.6; 131.1 (q, J = 32.9); 130.7; 129.2; 129.1; 128.7; 128.6; 125.2; 124.7; 72.8; 52.8; 44.7. FT- IR (cm^{-1}): 3253, 1713, 1635. MS/CI: $(M + H)^+$ 433 (m/z).

4.3. Microbiology. The biological activity of the synthesized compounds has been evaluated as reported elsewhere[24] toward *M. tuberculosis* H37Rv ATCC 27294.

■ ASSOCIATED CONTENT

Ⓢ Supporting Information

Tables S1-S10 and Figures S1-S17. This material is available free of charge via the Internet at http://pubs.acs.org.

■ AUTHOR INFORMATION

Corresponding Author

*E-mail: flavio.ballante@uniroma1.it (F.B.); rino.ragno@uniroma1.it (R.R.).

Author Contributions

§L.F. and F.B. contributed equally to this work

Notes

The authors declare no competing financial interest.

■ ACKNOWLEDGMENTS

We thank Dr. Roberto Cirilli (Dipartimento del Farmaco, Istituto Superiore di Sanità, Rome, Italy) for the chiral HPLC analysis. We also thank Prof. A. De Logu from "Dipartimento di Scienze e Tecnologie Biomediche", University of Cagliari, for the biological activity data. One of us (F.B.) acknowledge Sapienza Università di Roma (grant "Progetti per Avvio alla Ricerca" prot. C26N12JZCT).

■ REFERENCES

(1) WHO *Global tuberculosis report* 2012. http://www.who.int/tb/publications/global_report/en/index.html (accessed February 21, 2013).

(2) Ehlers, S. Lazy, dynamic or minimally recrudescent? On the elusive nature and location of the mycobacterium responsible for latent tuberculosis. *Infection* **2009**, *37*, 87−95.

(3) Di Perri, G.; Bonora, S. Which agents should we use for the treatment of multidrug-resistant Mycobacterium tuberculosis? *J. Antimicrob. Chemother.* **2004**, *54*, 593−602.

(4) Velayati, A. A.; Masjedi, M. R.; Farnia, P.; Tabarsi, P.; Ghanavi, J.; Ziazarifi, A. H.; Hoffner, S. E. Emergence of new forms of totally drug-resistant tuberculosis bacilli: super extensively drug-resistant tuberculosis or totally drug-resistant strains in iran. *Chest* **2009**, *136*, 420−425.

(5) Udwadia, Z. F.; Amale, R. A.; Ajbani, K. K.; Rodrigues, C. Totally drug-resistant tuberculosis in India. *Clin. Infect. Diseases* **2012**, *54*, 579−581.

(6) Guy, E. S.; Mallampalli, A. Managing TB in the 21st century: existing and novel drug therapies. *Ther. Adv. Respir. Dis.* **2008**, *2*, 401−408.

(7) Bhowruth, V.; Dover, L. G.; Besra, G. S. Tuberculosis chemotherapy: recent developments and future perspectives. *Prog. Med. Chem.* **2007**, *45*, 169−203.

(8) Piccaro, G.; Filippini, P.; Giannoni, F.; Scipione, L.; Tortorella, S.; De Vita, D.; Mellini, P.; Fattorini, L. Activity of drugs against dormant Mycobacterium tuberculosis. *J. Chemother.* **2011**, *23*, 175−178.

(9) Ragno, R.; Marshall, G. R.; Di Santo, R.; Costi, R.; Massa, S.; Rompei, R.; Artico, M. Antimycobacterial pyrroles: synthesis, anti-Mycobacterium tuberculosis activity and QSAR studies. *Bioorg. Med. Chem.* **2000**, *8*, 1423−1432.

(10) Biava, M.; Porretta, G. C.; Poce, G.; Supino, S.; Deidda, D.; Pompei, R.; Molicotti, P.; Manetti, F.; Botta, M. Antimycobacterial agents. Novel diarylpyrrole derivatives of BM212 endowed with high activity toward Mycobacterium tuberculosis and low cytotoxicity. *J. Med. Chem.* **2006**, *49*, 4946−4952.

(11) Ballante, F.; Ragno, R. 3-D QSAutogrid/R: an alternative procedure to build 3-D QSAR models. Methodologies and applications. *J. Chem. Inf. Model.* **2012**, *52*, 1674−1685.

(12) Manetti, F.; Corelli, F.; Biava, M.; Fioravanti, R.; Porretta, G. C.; Botta, M. Building a pharmacophore model for a novel class of antitubercular compounds. *Farmaco* **2000**, *55*, 484−491.

(13) Barnum, D.; Greene, J.; Smellie, A.; Sprague, P. Identification of common functional configurations among molecules. *J. Chem. Inf. Comput. Sci.* **1996**, *36*, 563−571.

(14) Biava, M.; Fioravanti, R.; Porretta, G. C.; Deidda, D.; Lampis, G.; Pompei, R.; Tafi, A.; Manetti, F. New derivatives of toluidine: Synthesis, antitubercular activity and pharmacophore hypothesis. *Med. Chem. Res.* **2002**, *11* (1), 50−66.

(15) Biava, M.; Porretta, G. C.; Poce, G.; De Logu, A.; Saddi, M.; Meleddu, R.; Manetti, F.; De Rossi, E.; Botta, M. 1,5-Diphenylpyrrole derivatives as antimycobacterial agents. Probing the influence on antimycobacterial activity of lipophilic substituents at the phenyl rings. *J. Med. Chem.* **2008**, *51*, 3644−8.

(16) Biava, M.; Porretta, G. C.; Deidda, D.; Pompei, R.; Tafi, A.; Manetti, F. Antimycobacterial compounds. New pyrrole derivatives of BM212. *Bioorg. Med. Chem.* **2004**, *12*, 1453−8.

(17) Biava, M.; Porretta, G. C.; Poce, G.; Deidda, D.; Pompei, R.; Tafi, A.; Manetti, F. Antimycobacterial compounds. Optimization of the BM 212 structure, the lead compound for a new pyrrole derivative class. *Bioorg. Med. Chem.* **2005**, *13*, 1221−30.

(18) Biava, M.; Cesare Porretta, G.; Deidda, D.; Pompei, R.; Tafi, A.; Manetti, F. Importance of the thiomorpholine introduction in new pyrrole derivatives as antimycobacterial agents analogues of BM 212. *Bioorg. Med. Chem.* **2003**, *11*, 515−20.

(19) Biava, M.; Porretta, G. C.; Poce, G.; De Logu, A.; Meleddu, R.; De Rossi, E.; Manetti, F.; Botta, M. 1,5-Diaryl-2-ethyl pyrrole derivatives as antimycobacterial agents: design, synthesis, and microbiological evaluation. *Eur. J. Med. Chem.* **2009**, *44*, 4734−8.

(20) Stammer, C. H.; Kartha, C. C.; Chaturvedi, N. C.; McKinney, J. D. Cycloserine derivatives. *J. Med. Chem.* **1970**, *13*, 1013−5.

(21) Feroci, M.; De Vita, D.; Scipione, L.; Sotgiu, G.; Tortorella, S. Electrogenerated acetonitrile anion induced selective N-alkylation of bifunctional compounds. *Tetrahedron Lett.* **2012**, *53*, 2564−2567.

(22) Jain, A. N. Ligand-based structural hypotheses for virtual screening. *J. Med. Chem.* **2004**, *47*, 947−61.

(23) Morris, G. M.; Huey, R.; Lindstrom, W.; Sanner, M. F.; Belew, R. K.; Goodsell, D. S.; Olson, A. J. AutoDock4 and AutoDockTools4: Automated docking with selective receptor flexibility. *J. Comput. Chem.* **2009**, *30*, 2785−91.

(24) Castagnolo, D.; De Logu, A.; Radi, M.; Bechi, B.; Manetti, F.; Magnani, M.; Supino, S.; Meleddu, R.; Chisu, L.; Botta, M. Synthesis, biological evaluation and SAR study of novel pyrazole analogues as inhibitors of Mycobacterium tuberculosis. *Bioorg. Med. Chem.* **2008**, *16*, 8587−91.